

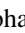



## Phase transition in the two-dimensional Heisenberg ferromagnet $\text{Fe}_3\text{GeTe}_2$ with long-range interaction

Ankita Tiwari <sup>1</sup>, Hyobin Ahn <sup>2</sup>, Birendra Kumar,<sup>1</sup> Jyoti Saini,<sup>1</sup> Pawan Kumar Srivastava,<sup>3</sup> Budhi Singh <sup>3</sup>, Changgu Lee,<sup>2,3</sup> and Subhasis Ghosh <sup>1,\*</sup>

<sup>1</sup>*School of Physical Sciences, Jawaharlal Nehru University, New Delhi-110067, India*

<sup>2</sup>*SKKU Advanced Institute of Nanotechnology (SAINT), Sungkyunkwan University, Suwon 16419, Republic of Korea*

<sup>3</sup>*School of Mechanical Engineering, Sungkyunkwan University, Suwon 16419, Republic of Korea*



(Received 21 August 2023; revised 1 December 2023; accepted 2 January 2024; published 25 January 2024)

We demonstrate that phase transition and continuous symmetry breaking can happen in  $2d$  Heisenberg ferromagnets with long range interaction in violation of the Hohenberg-Mermin-Wagner theorem. This has been possible to achieve in  $2d$  van der Waals ferromagnet  $\text{Fe}_3\text{GeTe}_2$  due to its exceptional tunability of magnetic properties. We argue that the variable critical exponent is a signature of phase transition in  $2d$  systems with long range ordering, consistent with recent results from density functional theory and quantum Monte Carlo calculations.

DOI: [10.1103/PhysRevB.109.L020407](https://doi.org/10.1103/PhysRevB.109.L020407)

In the last few decades, we have witnessed the amazing success of renormalization group (RG) theory of critical phenomena in explaining the universal behavior near continuous phase transition in a wide class of systems. So far, our understanding of universality classes (UCs) and universal behavior remains unchallenged in systems with short range (SR) interaction. However, the presence of long range (LR) interaction changes the scenario completely [1,2]. The most intriguing challenge comes from two aspects: (i) LR interaction driven violation of Goldstone theorem, thereby providing a mass to Goldstone modes, similar to the Higgs mechanism [3], and (ii) LR interaction driven violation of the Hohenberg-Mermin-Wagner (HMW) theorem facilitating, otherwise forbidden continuous symmetry breaking transitions in low dimension ( $d < 3$ ) [4,5]. In variance with SR driven universal behaviors in  $d < 3$ , LR interactions have been shown to be responsible for (i) interesting finite temperature transitions [6–8], (ii) new critical phenomena [1,9–12], (iii) continuously varying critical exponents in spin 1/2 Heisenberg systems [13–15], and (iv) continuous symmetry breaking in  $2d$  Rydberg array using a programmable quantum simulator [16,17]. Though it is realized that LR driven ferromagnetism is essential for circumventing HMW theorem in  $2d$ , experimental realization remains elusive in condensed matter systems.

A large number of experiments already exists in well-established  $2d$  systems, such as ultrathin magnetic films, atomic monolayer, and superconducting thin films [18–20], but the magnetic order and phase transition in these systems are predominantly governed by  $2d$  Ising,  $2d$  XY, and XY with fourfold anisotropy ( $\text{XYh}_4$ ) UCs which are governed by SR interaction. Moreover, there is always doubt about the low dimensionality ( $d < 3$ ) of these systems even in monolayer because bonding and hybridization with substrate are poorly

understood [21]. Recently, a new class of  $2d$  magnetic van der Waals (vdW) systems revolutionized condensed matter physics due to their exceptional magnetic properties [22,23]. It is possible that  $2d$  LR order, which was precluded in previously mentioned  $2d$  magnetic systems, make vdW  $2d$  ferromagnets most suitable to investigate the recently debated aforementioned issues in the context of LR order in  $2d$  magnetic systems [22,23].

In this Letter, we report how to break the limit of HMW theorem by providing experimental basis for  $2d$  Heisenberg ferromagnets in vdW systems. We have chosen vdW magnetic material  $\text{Fe}_3\text{GeTe}_2$  for following reasons. (i)  $\text{Fe}_3\text{GeTe}_2$  is  $2d$  layered material due to weak interlayer coupling with high Curie temperature ( $T_c$ )  $\sim 200$  K [24]. (ii)  $\text{Fe}_3\text{GeTe}_2$  hosts both localized and delocalized spins resulting itinerant and local-moment ferromagnetism [25–29], apparently due to LR and SR interactions, respectively. (iii)  $\text{Fe}_3\text{GeTe}_2$  is topologically constrained system exhibiting intriguing phenomena, such as anomalous Hall effect [30] and Kondo effect [31]. (iv) vdW bonding between layers in  $\text{Fe}_3\text{GeTe}_2$  results in highly anisotropic magnetic properties—the in plane spin-spin correlation length is much higher than that along the out of plane [26,32] and this is responsible for  $2d$  magnetism in bulk  $\text{Fe}_3\text{GeTe}_2$ , which provides a fertile system for studying the magnetism, and strong correlation in  $2d$  systems. Local-moment magnetism is governed by Heisenberg, Ising, or XY exchange interaction in  $d$  and  $f$  spins. The itinerant magnetism is primarily governed by LR Ruderman-Kittel-Kasuya-Yusida (RKKY) interaction in  $d$  and  $f$  electrons. Both itinerant and local-moment ferromagnets show Curie-Weiss law, however the microscopic origin is completely different. The Curie-Weiss law, temperature dependence of magnetic susceptibility, is governed by exchange interaction among localized spins in Heisenberg, Ising, or XY ferromagnets, and by nonlinear coupling among spin fluctuation modes in itinerant ferromagnets [33,34].

\*subhasis.ghosh.jnu@gmail.com

In a 2d LR Heisenberg model with power law decay couplings, the Hamiltonian  $\mathcal{H}$  for the ferromagnetic case can be given by  $\mathcal{H} = -\sum_{i \neq j} \frac{J}{|r_{ij}|^\alpha} \mathbf{S}_i \cdot \mathbf{S}_j$ , where  $J$  is strength of LR interaction, and the exponent  $\alpha$  distinguishes LR interaction from SR interaction and is generally represented by decay exponent  $\sigma$ , i.e.,  $\alpha = \sigma + d$ , where  $d$  is the dimension of the system [1]. Critical behavior with SR or LR interactions can be distinguished by a critical value of either  $\alpha$  ( $\alpha^*$ ) or  $\sigma$  ( $\sigma^*$ ). There are three different regions (i) for  $\sigma \leq d/2$  universal behavior which can be described by mean field model. (ii) For  $\sigma > \sigma^*$  or  $\alpha > \alpha^*$ , universal behavior is described by SR interaction based models. (iii) For  $d/2 < \sigma \leq \sigma^*$  or  $d < \alpha \leq \alpha^*$ , universal behavior can be described by LR interaction based models resulting in novel features like variable critical exponents [13–15], which has been shown here as a signature for 2d Heisenberg ferromagnet.

We have used single crystal of  $\text{Fe}_3\text{GeTe}_2$  grown by a chemical vapor transport method [35]. Details of sample growth is given in the Supplemental Material [36] (see also Refs. [37–56] therein). The single-crystalline crystallographic phase has been confirmed by single crystal x-ray diffraction (XRD). Magnetic measurements were carried out in the physical properties measurement system and detailed measurement protocol for temperature and field dependence of magnetization are given in the Supplemental Material [36]. XRD data for  $\text{Fe}_3\text{GeTe}_2$  is shown in Fig. 1. We found that crystal structure, space group, and lattice parameters are hexagonal,  $P6_3/mmc$ , and  $a = b = 4.022 \text{ \AA}$  and  $c = 16.387 \text{ \AA}$ , respectively. The XRD pattern of  $\text{Fe}_3\text{GeTe}_2$ , in which only (00l) [57] peaks are detected, indicates the surface of the crystal is parallel to the  $ab$  plane. Single crystals of  $\text{Fe}_3\text{GeTe}_2$  contains slabs of  $\text{Fe}_3\text{Ge}$  connected to vdW bonded Te atoms. Fe in  $\text{Fe}_3\text{GeTe}_2$  are in two inequivalent Wyckoff positions [58] and in the state of  $(\text{Fe}^{3+})_2\text{Fe}^{2+}\text{Ge}^{4+}(\text{Te}^{2-})_2$ , where Fe takes two different oxidation states, i.e.,  $\text{Fe}^{3+}$  and  $\text{Fe}^{2+}$ . Detailed crystal structure of  $\text{Fe}_3\text{GeTe}_2$  and its description is given in Fig. S1 of the Supplemental Material [36].

Temperature-dependent magnetization ( $M$ - $T$ ) for  $\text{Fe}_3\text{GeTe}_2$  with negligible Fe deficiency measured with field along  $\mu_0 H \parallel c$  and  $\mu_0 H \parallel ab$  is shown in Fig. 1. A large anisotropy by a factor of ten in magnetization between the  $ab$  plane and perpendicular to the  $ab$  plane indicates strong magnetism with large spin-spin correlation length in the  $ab$  plane. The phase transition from paramagnetic (PM) to ferromagnetic (FM) occurs at 223 K and is second order which has been ascertained by Landau analysis [59], entropy analysis [60], and Banerjee's criterion [61], discussed in Figs. S2, S3, and S4, respectively, in the Supplemental Material [36]. A kink around 160 K may be due to the additional magnetic interaction [62]. Further, field-dependent magnetization ( $M$ - $H$ ) taken at 10 K is shown in Fig. 1. Significant observations are as follows: (i) a clear hysteresis verifies the ferromagnetism in  $\text{Fe}_3\text{GeTe}_2$ ; (ii) until 5 T,  $M$  does not saturate but increases slowly with field; (iii) noninteger magnetic moment has been computed to be  $1.56 \mu_B/\text{Fe}$  at 5 T; (iv)  $T_c$  depends strongly on stoichiometry  $x$  in  $\text{Fe}_{3-x}\text{GeTe}_2$  [63] (Fig. S5 in the Supplemental Material [36]). Based on these observations and a plethora of first principle calculations backed by angle resolved photoemission and neutron scattering measurements, it has been established

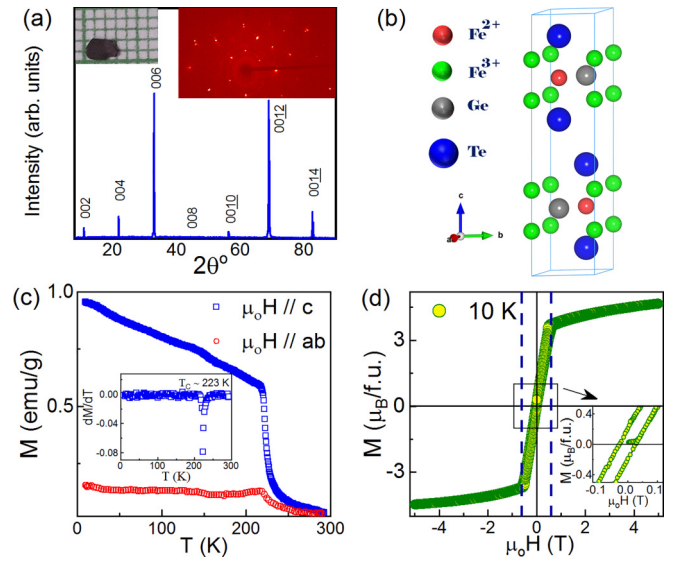


FIG. 1. (a) Single crystal XRD pattern for  $\text{Fe}_3\text{GeTe}_2$ , inset shows Laue pattern and image of single crystal. (b) Schematic representation of unit cell of  $\text{Fe}_3\text{GeTe}_2$ . Fe occupy two different Wyckoff positions [58]:  $\text{Fe}^{3+}$  and  $\text{Fe}^{2+}$ . (c)  $M$ - $T$  at an applied field  $\mu_0 H = 10 \text{ mT}$  for both  $\mu_0 H \parallel c$  and  $\mu_0 H \parallel ab$  [inset shows derivative of magnetization ( $dM/dT$ ), which gives minimum around  $\sim 223 \text{ K}$ , derivative done for  $\mu_0 H \parallel c$ ]. (d) Field-dependent magnetization ( $M$ - $H$ ) at 10 K.

beyond a doubt that  $\text{Fe}_3\text{GeTe}_2$  is ferromagnetic in which both localized and itinerant moments exist [25–29].

We should seek a different approach, relevant to magnetism and phase transition, in order to establish the itinerant magnetism in  $\text{Fe}_3\text{GeTe}_2$ . For itinerant ferromagnets, the Rhodes-Wohlfarth (RW) ratio is defined as  $P_c/P_s$  where  $P_c$  are numbers of magnetic carriers deduced from the Curie constant ( $C$ ) calculated from Fig. S6 in the Supplemental Material [36], where  $C = N_A \mu_B^2 P_{\text{eff}}^2 / 3k_B$ , and  $P_{\text{eff}} = \sqrt{P_c(P_c + 2)}$ .  $P_s$  are the number of magnetic carriers determined from saturation magnetization at low temperature [64,65]. For  $\text{Fe}_3\text{GeTe}_2$ ,  $P_s$  is calculated at 10 K. Figure 2 shows the field dependence of  $P_c/P_s$  which is greater than one even at high field suggesting that  $\text{Fe}_3\text{GeTe}_2$  has itinerant electrons and cannot be described only by localized moments.  $P_c/P_s$  decreases with field due to gradual crossover from itinerant magnetism to local moment driven magnetism at high fields. Hence, the effect of LR interaction can be controlled by field. This observation has been further corroborated by a generalized RW plot based on the spin fluctuations formalism put forward by Takahashi [66]. In this formalism the ratio  $T_c/T_o$  is an essential factor, which describes the level of itineracy of the spin moment, where  $T_o$  is the measure of spectral distribution in  $k$ -space, as itinerant electrons are localized in  $k$ -space [34]. Magnetic materials exhibit local moment magnetism at  $T_c/T_o \sim 1$ , but when  $T_c/T_o \ll 1$  the system has significant itinerant magnetism. The estimated value of  $T_c/T_o$  for  $\text{Fe}_3\text{GeTe}_2$  is 0.034 ( $T_o = 6524.87 \text{ K}$ , see Table S2 in the Supplemental Material [36]), which is close to the values reported for weak itinerant ferromagnets like  $\text{Sc}_3\text{In}$  (0.0097),  $\text{Ni}_3\text{Al}$  (0.0116), and  $\text{Au}_4\text{V}$  (0.17) [66–68]. The generalized RW relation  $P_{\text{eff}}/P_s$  vs  $T_c/T_o$  [66,70] is shown in Fig. S8 in the Supplemental Material [36];

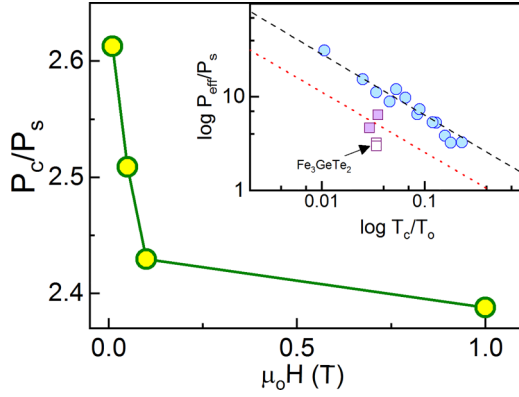


FIG. 2. RW plot for fields  $\mu_0 H = 0.01$  T,  $0.05$  T,  $0.1$  T, and  $1$  T. Solid line is a guide for eyes. Inset is the log-log plot of generalized RW plot. Solid circles are for  $3d$  and solid squares are for  $2d$  weak itinerant systems. Empty squares are for  $\text{Fe}_3\text{GeTe}_2$  plotted for fields  $\mu_0 H = 0.01$  T and  $1$  T. Data shown other than  $\text{Fe}_3\text{GeTe}_2$  are taken from Refs. [66–69]. Dash and dotted lines are the theoretical relation between  $P_{\text{eff}}/P_s$  and  $T_c/T_0$  for  $3d$  and  $2d$  weak itinerant systems, respectively, and adapted from Ref. [69].

the obtained value of  $P_{\text{eff}}/P_s$  is  $3.19$  and  $2.96$  for fields  $0.01$  T and  $1$  T, respectively. These values are lower than the values for  $3d$  systems as evidenced from the inset of Fig. 2. Detailed discussion on Takahashi formalism is given in the Supplemental Material [36]. Therefore it can be emphasized that  $\text{Fe}_3\text{GeTe}_2$  is a  $2d$  itinerant ferromagnet in which itinerancy can be controlled by an external field.

Figure 3 shows the  $M$ - $T$  taken at different fields ( $\mu_0 H = 0.01$  T,  $0.1$  T, and  $1$  T). It can be observed that  $M$ - $T$  does not show the usual  $T^{3/2}$  dependence as expected in  $3d$  Heisenberg ferromagnets with SR order [71]. The temperature dependence of magnetization variation  $\Delta M(T) = M(0) - M(T)$  due to thermal excitation of spin wave in Heisenberg ferromagnets diverges logarithmically [72] in  $2d$ , in accordance with HMW theorem. However, experimental observation of  $\Delta M(T)$  in  $2d$  can only be reconciled if LR ferromagnetic order is taken into account. It has been shown that the temperature dependence of  $M(T)$  due to LR ferromagnetic ordering in  $2d$  can be given by  $M(T) = M(0)[1 - aT \ln(bT)]$  [72–74], where  $a$  and  $b$  are constants decided by strength of exchange interaction, discussed in details in the Supplemental Material [36] and  $M(0)$  is the magnetization at  $T = 0$  K. Figure 3 shows the quasilinear dependence of  $M$  on temperature at different fields. For  $\mu_0 H = 0.01$  T and  $0.1$  T, the divergence from quasilinear behavior, according to the relation for  $M(T)$  explained above, occurs at  $50$  K and  $100$  K, beyond which magnetization due to itinerant spins dominates. When magnetic field increases to  $1$  T,  $M$ - $T$  shows quasilinear behavior in the entire low temperature region till the critical phenomena overrides the magnon dispersion near the phase transition, as the contribution from itinerant magnetization is minimized at higher field. The critical exponent  $\beta$  can be calculated directly from  $M$ - $T$  using the relation  $M_s(T) \propto (T_c - T)^\beta$ ,  $T < T_c$ . In Fig. 3, the  $\ln$ - $\ln$  plot of  $M$  vs  $T_c - T$  of  $M$ - $T$ , yields  $\beta$  values of  $0.468$  which is close to mean field UC at  $0.01$  T,  $0.447$  which is somewhere between mean field and Heisenberg UCs at  $0.1$  T, and  $0.388$  which is close to Heisenberg UC. As

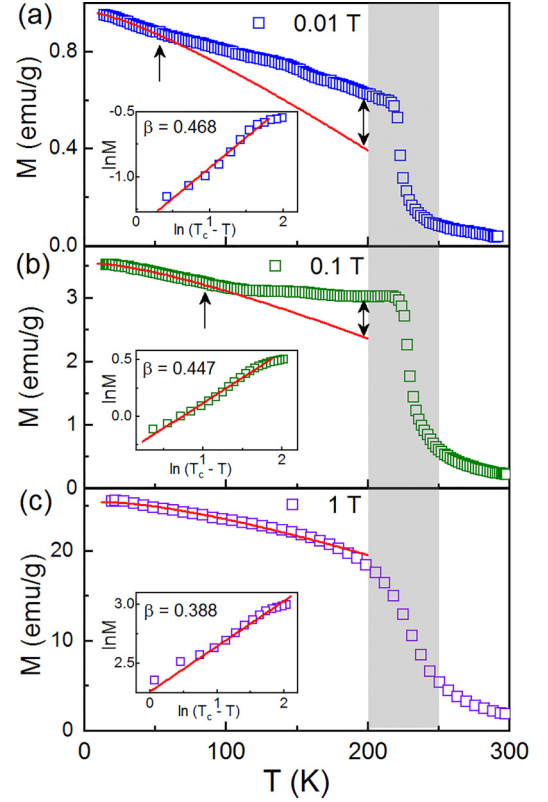


FIG. 3.  $M$ - $T$  at an applied field (a)  $\mu_0 H = 0.01$  T, (b)  $\mu_0 H = 0.1$  T, and (c)  $\mu_0 H = 1$  T. The solid lines in (a), (b), and (c) are fit to the data according to relation  $M(T) = M(0)[1 - aT \ln(bT)]$ . Inset of (a), (b), and (c) is  $\ln$ - $\ln$  of  $M$ - $T$ .  $\beta$  calculated from the gray shaded region, in the temperature range  $T = 215$  K– $231$  K,  $\Delta T = 1$  K. In inset red line is linear fit to the data.

mentioned before, for a spontaneous symmetry breaking in  $2d$  systems, there must be a LR interaction to override the HMW theorem [72]. Hence, the critical exponent for magnetic susceptibility,  $\gamma$  which is the most relevant for the range of interaction [1,9,15], needs to be analyzed precisely.

There are three issues to be resolved to reveal the physics: (i) How do the critical exponents depend on field? (ii) How do the critical exponents evolve when both delocalized and localized spins present in the system? And the most important issue is (iii) how to distinguish LR and SR interaction driven critical behavior? To resolve these issues and to achieve the main objective of this work, i.e., continuous symmetry breaking in a  $2d$  Heisenberg system induced by LR interaction, the critical isotherm and field dependent magnetic entropy change ( $\Delta S_M$ ) has been systematically investigated at  $T_c$ , (shown in Fig. S13 in the Supplemental Material [36]). The linear fit to the  $\ln$ - $\ln$  of  $M$  and  $\Delta S_M$  deviates at low and high fields. This indicates that the critical exponents depend on field. To confirm the appropriate UC and critical exponents, the Arrott-Noakes relation  $(\mu_0 H/M)^{1/\gamma} = (T - T_c)/T_c + (M/M')^{1/\beta}$ , where  $M'$  is temperature and field-independent constant, has been used by plotting  $(\mu_0 H/M)^{1/\gamma}$  vs  $(M/M')^{1/\beta}$ , known as modified Arrott plots (MAPs). MAPs are constructed from  $M$ - $H$  isotherms by using critical exponents  $\beta$  and  $\gamma$ . Over whole range of magnetic field ( $0.25$ – $5$  T) MAPs do not show parallel lines indicating variable critical exponents due to the presence of

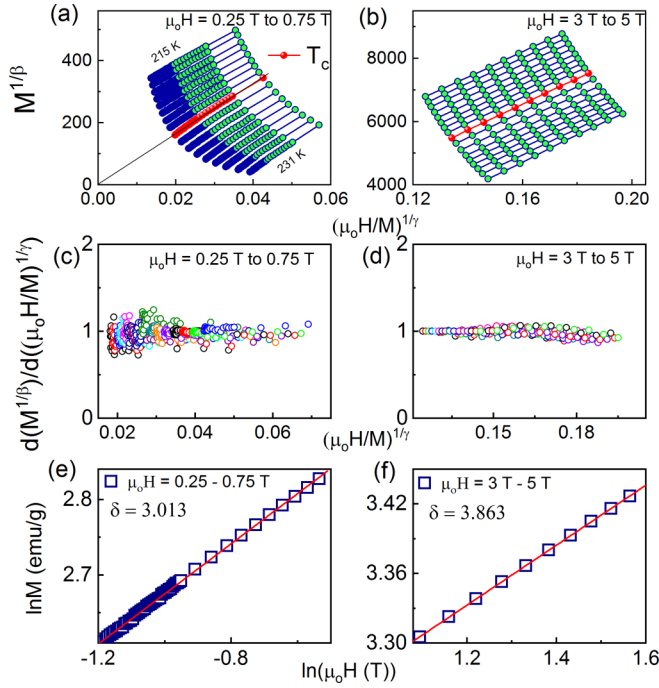


FIG. 4. MAPs for  $\text{Fe}_3\text{GeTe}_2$  constructed for field regions (a) 0.25 T–0.75 T, (b) 3 T–5 T. (c) and (d) shows derivative of MAPs for low and high field ranges. (e) and (f) shows the  $\delta$  values obtained at critical isotherm, solid line is the linear fit to the data.

LR interaction, as elaborated before. Critical exponents can only be determined accurately if MAPs show parallel straight lines which, so far, is ensured visually in literature. Here we show if the critical exponents depend on field, then it is impossible to get parallel straight lines in MAPs (discussed in Fig. S13 in the Supplemental Material [36]). To determine the critical exponents we have divided  $M$ - $H$  into four regions: (a) 0.25–0.75 T, (b) 0.75–1.5 T, (c) 1.5–3 T, and (d) 3–5 T. Using a rigorous iterative method as given in the details in the Supplemental Material [36], the exponents obtained for four field regions are  $\beta_1 = 0.500 \pm 0.004$  and  $\gamma_1 = 1.000 \pm 0.010$ ,  $\beta_2 = 0.439 \pm 0.006$  and  $\gamma_2 = 1.010 \pm 0.003$ ,  $\beta_3 = 0.388 \pm 0.001$  and  $\gamma_3 = 1.050 \pm 0.002$ , and  $\beta_4 = 0.384 \pm 0.001$  and  $\gamma_4 = 1.090 \pm 0.003$ , respectively. The field dependent MAPs for field range  $\mu_0 H = 0.25$ –0.75 T and  $\mu_0 H = 3$ –5 T is plotted in Fig. 4. The validity of the exponents can only be ensured if the derivative of the lines collapse to the line parallel to the  $x$  axis. Figure 4 shows  $d(M^{1/\beta})/d((\mu_0 H/M)^{1/\gamma})$  vs  $(\mu_0 H/M)^{1/\gamma}$  for  $\mu_0 H = 0.25$ –0.75 T and 3–5 T, respectively. The derivatives clearly collapse on to each other. The  $\delta$  has been calculated independently from critical isotherm for low and high field regions. The experimental  $\delta$  values match well with Widom scaling [75], further confirming the validity of the field dependent exponents. Figure S14 in the Supplemental Material [36] shows the MAPs for other field ranges. The set of exponents are listed in Table S4 in the Supplemental Material [36]. One can observe that as the field increases, the exponent  $\beta$  goes from mean field to Heisenberg like, i.e.,  $\beta$  goes from 0.500  $\rightarrow$  0.384, however  $\gamma$  remains close to one (varies from 1 to 1.09 as field increases), which suggests the presence of LR [9,15] in both cases of mean field dominated itinerant magnetism or exchange interaction dominated Heisenberg magnetism. We

further show that the validity of magnetic equation of state [76,77] can only be ensured in the case of field dependent critical exponents (Fig. S15 in the Supplemental Material [36]) and not in case of field independent critical exponents (Fig. S16 in the Supplemental Material [36]). So far, previous studies on critical behaviors in  $\text{Fe}_3\text{GeTe}_2$  resulted in ambiguous and diverse UCs. In Refs. [63,78,79], the values of  $\beta$  and  $\gamma$  have been claimed to be 0.372 and 1.265, 0.327 and 1.079, and 0.363 and 1.228 suggesting a combination of 3d Heisenberg and 3d XY, 3d Ising and MF, and 3d Heisenberg and 3d Ising, respectively. All these studies claimed  $\text{Fe}_3\text{GeTe}_2$  as a 3d system in variance with the fact that  $\text{Fe}_3\text{GeTe}_2$  is a 2d system. In the case of a monolayer grown either by exfoliation or epitaxially, a wide range of  $\beta$  values have been obtained based on limited analysis of critical behavior and UCs starting from mean field, 3d Heisenberg, 2d XY, and 2d Ising have been proposed without any emphasis on  $\gamma$  [24,25,80]. It is difficult to apprehend such a large variation on experimental results on monolayer  $\text{Fe}_3\text{GeTe}_2$ . There are several possibilities such as strong hybridization of substrate [21], effect of strain [81], and stoichiometry. More importantly, the 3d to 2d transition has been suggested on the proposition that  $T_c$  varies with the number of monolayers. However,  $T_c$  can also be varied by changing stoichiometry, i.e., by introducing vacancy at  $\text{Fe}^{2+}$  sites [63]. These ambiguities may have been stemmed from enforcing wrong dimension and range of interaction on critical analysis.

Finally, we discuss the range and dimensionality of spin-spin interaction using RG theory to further corroborate the appropriate UC with the help of critical exponents. Values of  $\sigma$  for different spatial and spin dimension are given in Table S5 in the Supplemental Material [36]. We found that  $\sigma < 1.5$  over the whole range of magnetic field. Hence, whether  $\beta = 0.5$  which is mean field, or  $\beta = 0.384$  which is close to Heisenberg UC,  $\gamma$  is close to one, and  $\sigma < 1.5$  and  $\alpha \in (2, 4)$ , emphasizing magnetic order and spontaneous symmetry breaking in  $\text{Fe}_3\text{GeTe}_2$ , driven by LR interaction. Recently, it has been shown [15] using large scale quantum Monte Carlo (QMC) simulations that there exists phase transition for  $\alpha \in (2, 4)$  in 2d Heisenberg ferromagnets with spontaneous  $\text{SU}(2)$  symmetry breaking. It has been further shown [15] that critical exponents for 2d Heisenberg ferromagnets are variable, i.e., function of  $\alpha$  or  $\sigma$ . Figure 5 shows how  $\beta$  and  $\gamma$  depends on  $\alpha$  which has been calculated for a different range of fields, as mentioned before. It is clear from Fig. 5 that  $\beta$  and  $\gamma$  qualitatively follow the theoretical results [15]. So far, RG analysis using classical field theory [9,10] predicted that there are three limits/ranges for  $\alpha$ , i.e., Gaussian fix point for  $2 < \alpha < 3$ , non-Gaussian fix point for  $3 < \alpha < 4$ , and absence of finite temperature ferromagnetism when  $\alpha \geq 4$ . These predictions have also been revisited using QMC simulations [15], and their finite size critical analysis satisfy both cases when the system is above critical dimension with Gaussian fix point ( $\alpha < 3$ ) and when the system is below the upper critical dimension ( $3 \leq \alpha < 4$ ). Hence, when  $\alpha \leq 3$ , the critical exponents are  $\gamma = 1$  and  $\beta = 0.5$  and when  $\alpha \geq 3$ ,  $\gamma \geq 1$ , and  $\beta \leq 0.5$ , which are observed in our experiments. As emphasized [15], the variable critical exponents and UC crossover differentiate 2d Heisenberg UCs from other UCs in 2d.

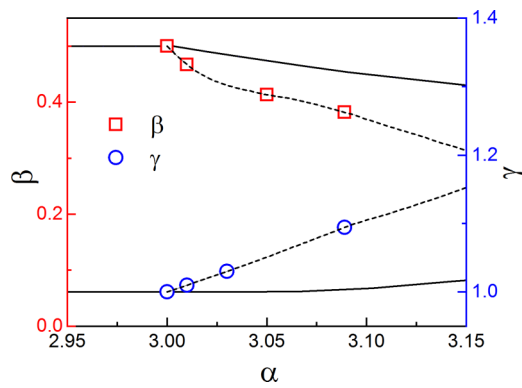


FIG. 5. Critical exponents  $\beta$  and  $\gamma$  plotted against  $\alpha = \sigma + d$ . Dashed lines are a guide for eyes. Solid lines are theoretical predictions [15] on how  $\beta$  and  $\gamma$  vary with  $\alpha$ . Symbol size takes care of the error.

Finally, we should discuss the possible microscopic origin of itinerant and local-moment magnetism in  $\text{Fe}_3\text{GeTe}_2$ . As mentioned before  $\text{Fe}_3\text{GeTe}_2$  has two inequivalent charge states of Fe,  $\text{Fe}^{2+}$ , and  $\text{Fe}^{3+}$ , resulting in a multiorbital path for different spin-spin interactions. In the case of a hexagonal crystal field, as in  $\text{Fe}_3\text{GeTe}_2$ , the five  $3d$  orbitals of the Fe atom split into a three group of orbitals,  $a_1$  ( $d_{z^2}$ ), two twofold-degenerate states  $e_1$  ( $d_{x^2-y^2}$  and  $d_{xy}$ ), and  $e_2$  ( $d_{xz}$  and  $d_{yz}$ ). DFT calculations [26–29,82] show that the  $a_1$  ( $d_{z^2}$ ) and  $e_2$  ( $d_{xz}$  and  $d_{yz}$ ) orbitals are narrower and localized compared to orbital  $e_1$  ( $d_{x^2-y^2}$  and  $d_{xy}$ ) which is wider and delocalized. Hence, there would be two types of exchange mechanisms, i.e., the itinerant magnetism with  $e_1$  electrons and the local-moment

magnetism with  $a_1$  and  $e_2$  orbitals. It has been shown [27] that  $d_{x^2-y^2}/d_{xy}$  electrons lie close to Fermi level, and contribute to the itinerant ferromagnetism in  $\text{Fe}_3\text{GeTe}_2$ . We argue that, as field increases more and more delocalized electrons are polarized weakening itinerant magnetism without any effect on localized electrons responsible for local-moment Heisenberg magnetism.

In conclusion, we have presented detailed experimental evidences for  $2d$  Heisenberg ferromagnetism by breaking the HMW limit. This has been possible due to exceptional tunability of magnetic properties of  $\text{Fe}_3\text{GeTe}_2$ . The presence of both itinerant and local-moment magnetism in  $\text{Fe}_3\text{GeTe}_2$  has facilitated to reveal variable critical exponents. Temperature dependence of magnetization, RW, and generalized RW based analysis established that  $\text{Fe}_3\text{GeTe}_2$  is a  $2d$  ferromagnet with itinerant magnetism which can be tuned by magnetic field. The critical exponents determined by an improvised method unambiguously show that the exponent  $\gamma$  reveals LR interaction over the wide range of field, but the exponent  $\beta$  crosses from mean field UC to  $2d$  Heisenberg UC as field increases. We argue that variable critical exponents is a signature of  $2d$  Heisenberg ferromagnetism, as emphasized by recent theoretical calculations. Multiorbital character in  $\text{Fe}_3\text{GeTe}_2$  provides the underlying LR ordering for both itinerant and local-moment ferromagnetism.

A.T. acknowledges UGC, India for financial support through fellowship. This project is partially supported by SERB (Project No. CRG/2021/000776) and the FIST program of DST, Govt. of India and Samsung Research Funding Center of Samsung Electronics (Project No. SRFC-MA2102-02).

- [1] N. Defenu, T. Donner, T. Macrì, G. Pagano, S. Ruffo, and A. Trombettoni, *Rev. Mod. Phys.* **95**, 035002 (2023).
- [2] A. Campa, T. Dauxois, D. Fanelli, and S. Ruffo, *Physics of Long-Range Interacting Systems* (Oxford University Press, Oxford, UK, 2014).
- [3] O. K. Diessel, S. Diehl, N. Defenu, A. Rosch, and A. Chiocchetta, *Phys. Rev. Res.* **5**, 033038 (2023).
- [4] N. D. Mermin and H. Wagner, *Phys. Rev. Lett.* **17**, 1133 (1966).
- [5] P. C. Hohenberg, *Phys. Rev.* **158**, 383 (1967).
- [6] M. Weber, D. J. Luitz, and F. F. Assaad, *Phys. Rev. Lett.* **129**, 056402 (2022).
- [7] Z. Li, S. Choudhury, and W. V. Liu, *Phys. Rev. A* **104**, 013303 (2021).
- [8] D. Peter, S. Müller, S. Wessel, and H. P. Büchler, *Phys. Rev. Lett.* **109**, 025303 (2012).
- [9] M. E. Fisher, S.-K. Ma, and B. G. Nickel, *Phys. Rev. Lett.* **29**, 917 (1972).
- [10] J. Sak, *Phys. Rev. B* **8**, 281 (1973).
- [11] J. A. Koziol, A. Langheld, S. C. Kapfer, and K. P. Schmidt, *Phys. Rev. B* **103**, 245135 (2021).
- [12] S. Fey, S. C. Kapfer, and K. P. Schmidt, *Phys. Rev. Lett.* **122**, 017203 (2019).
- [13] P. Adelhardt and K. P. Schmidt, *SciPost Phys.* **15**, 087 (2023).
- [14] N. Khan, P. Sarkar, A. Midya, P. Mandal, and P. K. Mohanty, *Sci. Rep.* **7**, 45004 (2017).
- [15] J. Zhao, M. Song, Y. Qi, J. Rong, and Z. Y. Meng, *npj Quantum Mater.* **8**, 59 (2023).
- [16] P. Scholl, M. Schuler, H. J. Williams, A. A. Eberharter, D. Barredo, K.-N. Schymik, V. Lienhard, L.-P. Henry, T. C. Lang, T. Lahaye *et al.*, *Nature (London)* **595**, 233 (2021).
- [17] C. Chen, G. Bornet, M. Bintz, G. Emperauger, L. Leclerc, V. S. Liu, P. Scholl, D. Barredo, J. Hauschild, S. Chatterjee *et al.*, *Nature (London)* **616**, 691 (2023).
- [18] A. Taroni, T. Bramwell, and P. Holdsworth, *J. Phys.: Condens. Matter* **20**, 275233 (2008).
- [19] C. A. F. Vaz, J. A. C. Bland, and G. Lauthoff, *Rep. Prog. Phys.* **71**, 056501 (2008).
- [20] F. Hellman, A. Hoffmann, Y. Tserkovnyak, G. S. D. Beach, E. E. Fullerton, C. Leighton, A. H. MacDonald, D. C. Ralph, D. A. Arena, H. A. Dürr *et al.*, *Rev. Mod. Phys.* **89**, 025006 (2017).
- [21] A. Bedoya-Pinto, J.-R. Ji, A. K. Pandeya, P. Gargiani, M. Valvidares, P. Sessi, J. M. Taylor, F. Radu, K. Chang, and S. S. P. Parkin, *Science* **374**, 616 (2021).
- [22] K. S. Burch, D. Mandrus, and J.-G. Park, *Nature (London)* **563**, 47 (2018).
- [23] Q. H. Wang, A. Bedoya-Pinto, M. Blei, A. H. Dismukes, A. Hamo, S. Jenkins, M. Koperski, Y. Liu, Q.-C. Sun, E. J. Telford *et al.*, *ACS Nano* **16**, 6960 (2022).

- [24] Y. Deng, Y. Yu, Y. Song, J. Zhang, N. Z. Wang, Z. Sun, Y. Yi, Y. Z. Wu, S. Wu, J. Zhu *et al.*, *Nature (London)* **563**, 94 (2018).
- [25] Z. Fei, B. Huang, P. Malinowski, W. Wang, T. Song, J. Sanchez, W. Yao, D. Xiao, X. Zhu, A. F. May *et al.*, *Nat. Mater.* **17**, 778 (2018).
- [26] S. Bao, W. Wang, Y. Shangguan, Z. Cai, Z.-Y. Dong, Z. Huang, W. Si, Z. Ma, R. Kajimoto, K. Ikeuchi *et al.*, *Phys. Rev. X* **12**, 011022 (2022).
- [27] X. Bai, F. Lechermann, Y. Liu, Y. Cheng, A. I. Kolesnikov, F. Ye, T. J. Williams, S. Chi, T. Hong, G. E. Granroth *et al.*, *Phys. Rev. B* **106**, L180409 (2022).
- [28] Q. Liu, J. Xing, Z. Jiang, Y. Guo, X. Jiang, Y. Qi, and J. Zhao, *Commun. Phys.* **5**, 140 (2022).
- [29] T. J. Kim, S. Ryee, and M. J. Han, *Npj Comput. Mater.* **8**, 245 (2022).
- [30] K. Kim, J. Seo, E. Lee, K.-T. Ko, B. S. Kim, B. G. Jang, J. M. Ok, J. Lee, Y. J. Jo, W. Kang *et al.*, *Nat. Mater.* **17**, 794 (2018).
- [31] Y. Zhang, H. Lu, X. Zhu, S. Tan, W. Feng, Q. Liu, W. Zhang, Q. Chen, Y. Liu, X. Luo *et al.*, *Sci. Adv.* **4**, eaao6791 (2018).
- [32] C. Tan, J. Lee, S.-G. Jung, T. Park, S. Albarakati, J. Partridge, M. R. Field, D. G. McCulloch, L. Wang, and C. Lee, *Nat. Commun.* **9**, 1554 (2018).
- [33] T. Moriya, *Spin Fluctuations in Itinerant Electron Magnetism* (Springer, Berlin, Heidelberg, 1985), pp. 194–213.
- [34] Y. Takahashi, *Spin Fluctuation theory of Itinerant Electron Magnetism* (Springer, Berlin, Heidelberg, 2013), Vol. 9.
- [35] B. Chen, J. Yang, H. Wang, M. Imai, H. Ohta, C. Michioka, K. Yoshimura, and M. Fang, *J. Phys. Soc. Jpn.* **82**, 124711 (2013).
- [36] See Supplemental Material at <http://link.aps.org/supplemental/10.1103/PhysRevB.109.L020407> for the details of crystal growth, crystal structure, magnetic measurements and protocol, order of phase transition; details of itinerant analysis from which Fig. 2 of main article has been made; detailed critical analysis from which Figs. 4 and 5 of main article has been made; spin interaction and renormalization group approach. The Supplemental Material also contains Refs. [37–56].
- [37] H. C. Chauhan, B. Kumar, J. K. Tiwari, and S. Ghosh, *Phys. Rev. B* **100**, 165143 (2019).
- [38] C. Romero-Muñiz, R. Tamura, S. Tanaka, and V. Franco, *Phys. Rev. B* **94**, 134401 (2016).
- [39] C. M. Bonilla, J. Herrero-Albillos, F. Bartolomé, L. M. García, M. Parra-Borderías, and V. Franco, *Phys. Rev. B* **81**, 224424 (2010).
- [40] L. Xu, J. Fan, Y. Zhu, Y. Shi, L. Zhang, L. Pi, Y. Zhang, and D. Shi, *Mater. Res. Bull.* **73**, 187 (2016).
- [41] J. Yang, B. Chen, H. Wang, Q. Mao, M. Imai, K. Yoshimura, and M. Fang, *Phys. Rev. B* **88**, 064406 (2013).
- [42] T. Kanomata, T. Igarashi, H. Nishihara, K. Koyama, K. Watanabe, K. U. Neumann, and K. R. A. Ziebeck, *Mater. Trans.* **47**, 496 (2006).
- [43] B. Chen, H. Ohta, C. Michioka, and K. Yoshimura, *J. Phys. Soc. Jpn.* **79**, 064707 (2010).
- [44] Y. Takahashi, *J. Phys.: Condens. Matter* **13**, 6323 (2001).
- [45] K. Koyama, H. Sasaki, T. Kanomata, K. Watanabe, and M. Motokawa, *J. Phys. Soc. Jpn.* **72**, 767 (2003).
- [46] H. Ohta and K. Yoshimura, *Phys. Rev. B* **79**, 184407 (2009).
- [47] W. Dürr, M. Taborelli, O. Paul, R. Germar, W. Gudat, D. Pescia, and M. Landolt, *Phys. Rev. Lett.* **62**, 206 (1989).
- [48] U. Gradmann, M. Przybylski, H. J. Elmers, and G. Liu, *Appl. Phys. A* **49**, 563 (1989).
- [49] M. E. Fisher, *Rev. Mod. Phys.* **46**, 597 (1974).
- [50] J. Fan, L. Ling, B. Hong, L. Zhang, L. Pi, and Y. Zhang, *Phys. Rev. B* **81**, 144426 (2010).
- [51] M. E. Fisher, *Rep. Prog. Phys.* **31**, 418 (1968).
- [52] A. Arrott and J. E. Noakes, *Phys. Rev. Lett.* **19**, 786 (1967).
- [53] L. Zhang, J. Fan, X. Zhu, W. Ning, Z. Qu, M. Ge, L. Pi, and Y. Zhang, *Appl. Phys. A* **113**, 201 (2013).
- [54] J. S. Kouvel and M. E. Fisher, *Phys. Rev.* **136**, A1626 (1964).
- [55] S. F. Fischer, S. N. Kaul, and H. Kronmüller, *Phys. Rev. B* **65**, 064443 (2002).
- [56] J. K. Tiwari, H. C. Chauhan, B. Kumar, and S. Ghosh, *J. Phys.: Condens. Matter* **32**, 195803 (2020).
- [57] A. F. May, S. Calder, C. Cantoni, H. Cao, and M. A. McGuire, *Phys. Rev. B* **93**, 014411 (2016).
- [58] H.-J. Deiseroth, K. Aleksandrov, C. Reiner, L. Kienle, and R. K. Kremer, *Eur. J. Inorg. Chem.* **2006**, 1561 (2006).
- [59] J. C. Tolédano and P. Tolédano, *The Landau Theory of Phase Transitions* (World Scientific, Singapore, 1987).
- [60] V. Franco, A. Conde, J. M. Romero-Enrique, and J. S. Blázquez, *J. Phys.: Condens. Matter* **20**, 285207 (2008).
- [61] B. Banerjee, *Phys. Lett.* **12**, 16 (1964).
- [62] J. Yi, H. Zhuang, Q. Zou, Z. Wu, G. Cao, S. Tang, S. A. Calder, P. R. C. Kent, D. Mandrus, and Z. Gai, *2D Mater.* **4**, 011005 (2016).
- [63] Y. Liu, V. N. Ivanovski, and C. Petrovic, *Phys. Rev. B* **96**, 144429 (2017).
- [64] E. P. Wohlfarth, *J. Magn. Magn. Mater.* **7**, 113 (1978).
- [65] T. Moriya, *J. Magn. Magn. Mater.* **14**, 1 (1979).
- [66] Y. Takahashi, *J. Phys. Soc. Jpn.* **55**, 3553 (1986).
- [67] J. Takeuchi and Y. Masuda, *J. Phys. Soc. Jpn.* **46**, 468 (1979).
- [68] F. R. de Boer, C. J. Schinkel, J. Biesterbos, and S. Proost, *J. App. Phys.* **40**, 1049 (1969).
- [69] M. Imai, C. Michioka, H. Ueda, and K. Yoshimura, *Phys. Rev. B* **91**, 184414 (2015).
- [70] K. Shimizu, H. Maruyama, H. Yamazaki, and H. Watanabe, *J. Phys. Soc. Jpn.* **59**, 305 (1990).
- [71] N. W. Ashcroft and N. D. Mermin, *Solid State Physics* (Saunders college, Philadelphia, 1976).
- [72] P. Bruno, *Phys. Rev. B* **43**, 6015 (1991).
- [73] R. Skomski, *Simple Models of Magnetism* (Oxford University Press, Oxford, UK, 2008).
- [74] M. J. Klein and R. S. Smith, *Phys. Rev.* **81**, 378 (1951).
- [75] L. P. Kadanoff, *Phys. Phys. Fiz.* **2**, 263 (1966).
- [76] S. N. Kaul, *J. Magn. Magn. Mater.* **53**, 5 (1985).
- [77] H. E. Stanley, *Rev. Mod. Phys.* **71**, S358 (1999).
- [78] B. Liu, Y. Zou, S. Zhou, L. Zhang, Z. Wang, H. Li, Z. Qu, and Y. Zhang, *Sci. Rep.* **7**, 6184 (2017).
- [79] Q. Mao, B. Chen, J. Yang, Y. Zhang, H. Wang, and M. Fang, *J. Phys.: Condens. Matter* **30**, 345802 (2018).
- [80] S. Liu, X. Yuan, Y. Zou, Y. Sheng, C. Huang, E. Zhang, J. Ling, Y. Liu, W. Wang, C. Zhang *et al.*, *npj 2D Mater. Appl.* **1**, 30 (2017).
- [81] X. Hu, Y. Zhao, X. Shen, A. V. Krashennnikov, Z. Chen, and L. Sun, *ACS Appl. Mater. Interfaces* **12**, 26367 (2020).
- [82] J.-X. Zhu, M. Janoschek, D. S. Chaves, J. C. Cezar, T. Durakiewicz, F. Ronning, Y. Sassa, M. Mansson, B. L. Scott, N. Wakeham *et al.*, *Phys. Rev. B* **93**, 144404 (2016).